Supplementary Information to "Fluctuation induced network patterns in active matter with spatially correlated noise "

Sebastian Fehlinger, Kai Cui, Arooj Sajjad, Heinz Koeppl and Benno Liebchen

1 Correlated random fields

We use the method described in [1, 2, 3]. That is, we start with a Gaussian white noise field with zero mean and unit variance $\phi_{\text{white}}(\vec{r})$. The second step is to Fourier transform this field to get $\tilde{\phi}_{\text{white}}(\vec{k})$. As a third step, we choose $P(\vec{k}) = |\vec{k}|^{-\alpha}$. Finally, we define $\tilde{\phi}(\vec{k}) = P^{1/2}(\vec{k})\tilde{\phi}_{\text{white}}(\vec{k})$ and do the inverse Fourier transformation to get the correlated field $\phi(\vec{r})$ in real space. We note, that when defining $\tilde{\phi}(\vec{k})$ in this way, $P(\vec{k})$ is the Fourier transform of the correlation function $C(\vec{r},\vec{r}') = \langle\phi(\vec{r})\phi(\vec{r}')\rangle$, which shows, that the random field exhibits a characteristic distribution of correlation lengths, that is determined by the chosen power law exponent α. Thus, the larger the value of α, the stronger is the presence of longer ranged correlations in $\phi(\vec{r})$. To guarantee periodic boundary conditions, we choose $\vec{k} = \frac{2\pi\vec{r}}{L}$. Numerically, we generate a lattice on our simulation box of size $L \times L$. The distance between two lattice sites is equal to the particle diameter σ (which is sufficient in the absence of temporal correlations of ϕ). Then, for every grid point we draw a random number from a Gaussian distribution with zero mean and unit variance (white noise). After the Fourier transformation (using the FFTW package in C [4]), these random numbers are multiplied with the square root of the power spectrum before using the inverse Fourier transformation to get back to real space.
For each particle, we evaluate the random field at the gridpoint that is closest to its momentaneous position. Together with volume exclusion interactions between the particles, our choice of the grid spacing ensures, that neighbouring particles do not experience identical random forces. In addition, since the noise field varies very slowly in space compared to the particle size, interpolation of the random forces at adjacent grid points would not relevantly change our results. Different realizations of the field for different α are shown in Fig. 1 in the main text.

2 Numerical simulations

For solving the equations of motions we use a straight forward Euler-Maruyama scheme, which is reasonable, since the spatially correlated random field is uncorrelated in time, so $\langle\phi(\vec{r}^*,t^*)\phi(\vec{r}^*,t^{*\prime})\rangle \sim \delta(t^*-t^{*\prime})$. The time discretized equations are (already in dimensionless units as in the main text)

$$\vec{r}_i^*(t^*+\Delta t^*) = \vec{r}_i^*(t^*) + \hat{n}_i(t^*)\Delta t^* - \Delta t^*\nabla_{r^*}U^*(r^*)$$
$$\theta_i^*(t^*+\Delta t^*) = \theta_i^*(t^*) + \omega^*\Delta t^* + \Delta t^*\kappa^*\sum_{j\in\partial_i}\sin(\theta_j^*-\theta_i^*) + \sqrt{\Delta t^*}a^*\phi_\alpha(\vec{r}_i^*,t^*).$$

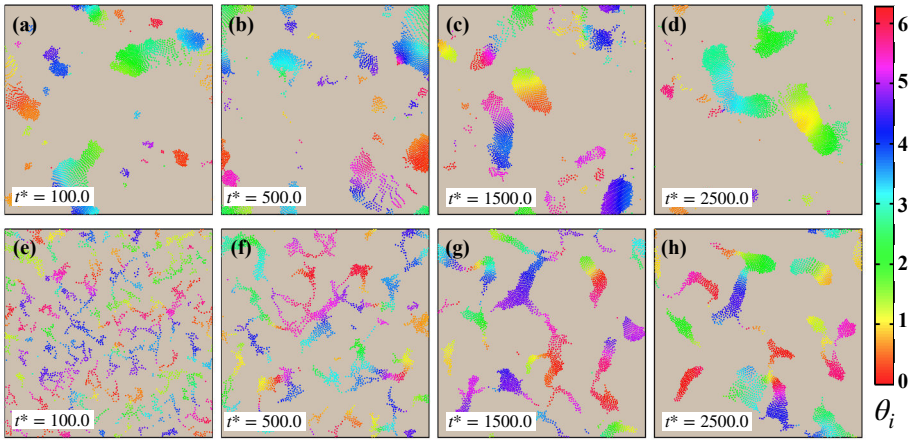

Figure S1: Snapshots for $N = 2500$ particles and a correlated random field with $\alpha = 4.0$. The colorbar indicates the orientation θ_i of each particle. (a)-(d) For $\omega^* = 0.0$ we observe flocking as described by the Viscek model. The spatial correlations sometimes pull particles within a flock apart from each other. (e)-(h) Increasing the rotational frequency to $\omega^* = 1.0$ leads to the formation of elongated structures which build again flocks for longer times. Other parameters are: $\Phi_0 = 0.1$, $\kappa^* = 1.0$, $\epsilon^* = 1.0$ and $a^* = 1.0$.

In all simulations we use a time step of $\Delta t^* = 10^{-5}$.

2.1 Flocking behavior

As already discussed in the main text, for comparatively small rotational frequencies, the system shows flocking, similarly as in the Viscek model, see Fig. S1 for snapshots.

2.2 Robustness of network patterns against additional Gaussian white noise

To test the robustness of the network patterns (Fig. 2 in the main text) against thermal fluctuations, we now include additional Gaussian white noise in the equations of motion of all particles, which corresponds to $D, D_r \neq 0$ in Eqs. (1),(2) in the main text. In dimensionless form, the equations now read:

$$\dot{\vec{r}}_i^*(t^*) = \hat{n}_i(t^*) - \nabla_{r^*} U^*(r^*) + b^* \vec{\eta}_i(t^*)$$
$$\dot{\theta}_i^*(t^*) = \omega^* + \kappa^* \sum_{j \in \partial_i} \sin(\theta_j^* - \theta_i^*) + a^* \phi_\alpha(\vec{r}_i^*, t^*) + c^* \xi_i(t^*),$$

where $\vec{\eta}$ and ξ describe white noise with zero mean and unit variance with parameters $b^* = \sqrt{\frac{2D}{\sigma v_0}}$ and $c^* = \sqrt{\frac{2D_r \sigma}{v_0}}$. Fig. S2(a)-(d) shows snapshots for $b^* = 0.01$ and $c^* = 0.1$. Other parameters are as in Fig. 2 in the main text, i.e. $\omega^* = 3.0$ and $\alpha = 4.0$).

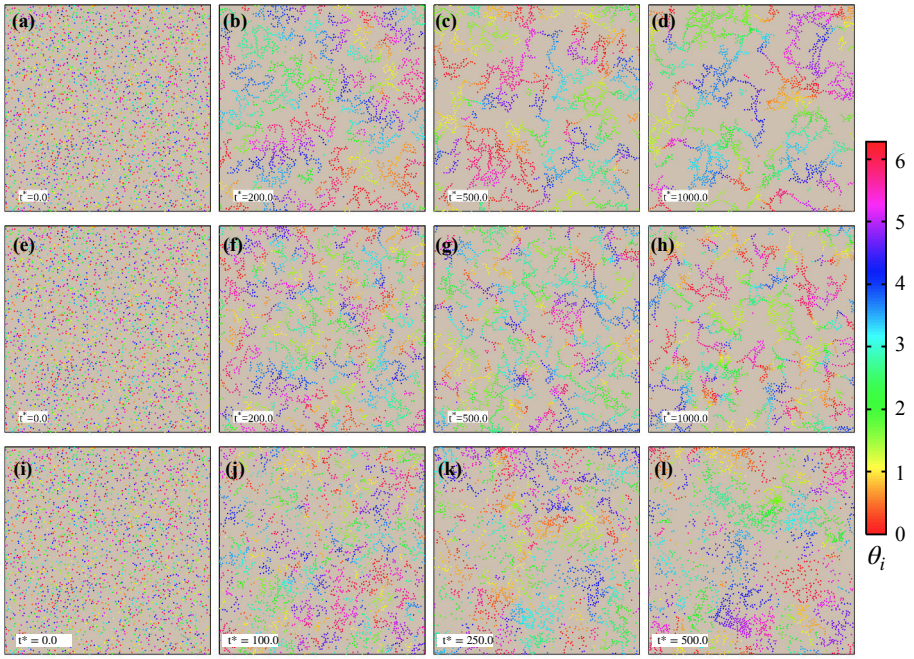

Figure S2: (a)-(d) Simulation snapshots with additional Gaussian white noise, where $b^* = 0.01$ and $c^* = 0.1$. (e)-(h) Snapshots of a simulation, where the spatially correlated but temporally uncorrelated random field also acts on the center of mass coordinates of the particles. Here, the amplitude of this additional field is $d^* = 0.2$. (i)-(l) Simulation snapshots for a random field that acts only on the center of mass coordinate of the particles and not on the orientation ($a^* = 0.0$ and $d^* = 1.0$). As in the main text, the color coding indicates the particle's orientation. Further parameters in both cases are: $\omega^* = 3.0$, $\alpha = 4.0$, $\kappa^* = 1.0$, $\epsilon^* = 1.0$, $a^* = 1.0$ and $\Phi_0 = 0.1$.

2.3 Robustness of network patterns against correlated noise acting on the center of mass coordinate

Further we explore the influence of correlated random fields acting on the center of mass coordinate $\vec{r}_i^*$ of the particles. Therefore, we introduce three different Gaussian random fields $\phi_{\alpha,x}$, $\phi_{\alpha,y}$ and $\phi_{\alpha,\theta}$ with identical correlation exponent α, leading to the following equations of motion:

$$\dot{\vec{r}}_i^* = \hat{n}_i(t^*) - \nabla_{r^*} U^*(r^*) + d^* \vec{\phi}_\alpha(\vec{r}^*, t^*)$$
$$\dot{\theta}_i^* = \omega^* + \kappa^* \sum_{j \in \partial_i} \sin(\theta_j^* - \theta_i^*) + a^* \phi_{\alpha,\theta}(\vec{r}_i^*, t^*).$$

Here, $\vec{\phi}_\alpha = (\phi_{\alpha,x}, \phi_{\alpha,y})$ and again, we neglect thermal fluctuations. Fig. S2(e)-(h) shows snapshots for $d^* = 0.2$, $\omega^* = 3.0$ and $\alpha = 4.0$. We clearly see that the network patterns which we discuss in the main text, persist in the presence of additional noise terms. When further increasing the strength of these additional noise terms, at some point, the network patterns cease to exist. Additionally,

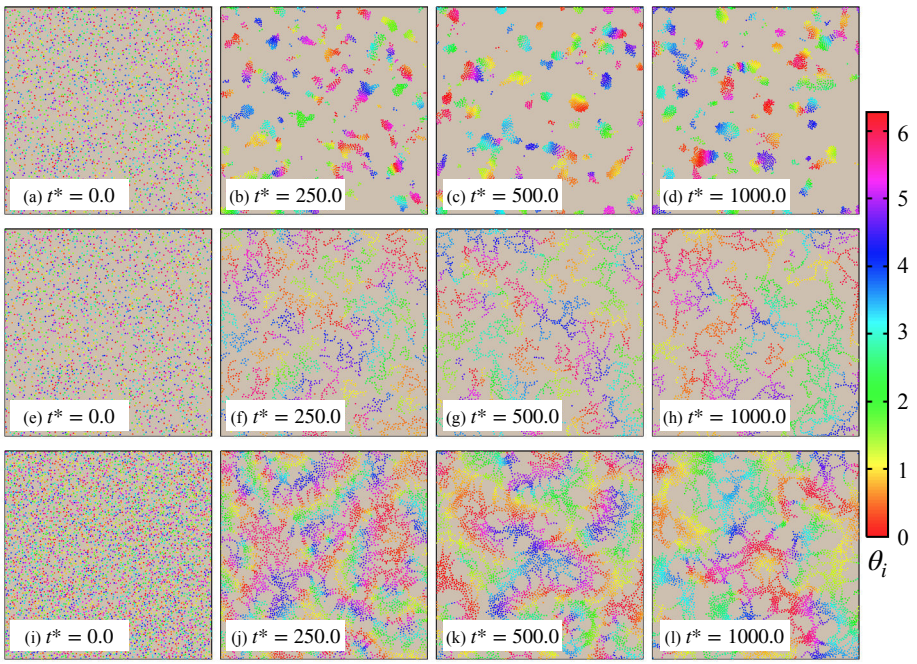

Figure S3: Simulation snapshots for the same parameters as in Fig. 2(a)-(d) of the main text, i.e. for $\omega^* = 3.0$, $\alpha = 4.0$, $\epsilon^* = 1.0$, $\kappa^* = 1.0$ and $\Phi_0 = 0.1$, but with an enhanced amplitude of the random field $a^* = 5.0$ ((a)-(d)), an enhanced alignment strength $\kappa^* = 10.0$ ((e)-(h)) and an enhanced packing fraction $\Phi_0 = 0.2$ ((i)-(l)). Colors indicate particle orientations.

we simulate the case, where the correlated random field only acts on the center of mass coordinate of the particles and not on their orientations and we do not observe the emergence of network patterns (see Fig. S2(i)-(l) for snapshots).

2.4 Role of alignment strength, amplitude of the random field and packing fraction

Here we further explore the network patterns by exemplary varying additional parameters. Fig. S3 shows that the network patterns persist when enhancing the alignment strength or the density, but they do not form when strongly enhancing the amplitude of the correlated noise field. That is, network patterns require some correlated noise to emerge, but they cease to exist when the fluctuations are too large.

2.5 Role of short-range repulsions

Finally, we explore the influence of volume exclusion interactions between the particles. Therefore, we perform simulations with $\epsilon^* = 0$ and find, that also in that case, network patterns occur (see Fig. S4).

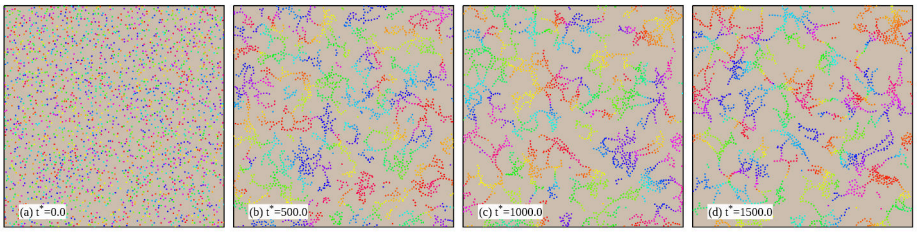

Figure S4: (a)-(d) Simulation snapshots without steric volume exclusion ($\epsilon^* = 0$). Colors indicate particle orientations as in Fig. S2. Further parameters are: $\omega^* = 3.0$, $\alpha = 4.0$, $\kappa^* = 1.0$, $a^* = 1.0$ and $\Phi_0 = 0.1$.

3 Counting holes within a network pattern

For calculating the number of holes in a network pattern (as shown in Fig. 3 in the main text), we divide the simulation box into bins with a width of two particle diameters and check for each bin, if it contains a particle or not. Then we use the bwlabel command of MATLAB (adopted to account for periodic boundary conditions) to find all neighboring bins, which are empty. Finally, we delete the largest hole which is essentially the environment of the pattern. Further we introduce a minimal hole size of two bins.

4 Construction of persistence diagrams

In Fig. S5 we illustrate how we construct persistence diagrams from the particle positions.

5 Characteristic timescales

The physical mechanism underlying the emergence of network patterns, as described in the main text, depends on the fact that the lifetime of dimers τ_c is long compared to the average attachment time τ_a for an additional particle to attach to a dimer. To estimate τ_a, in our simulations we first calculate the number of dimers during the simulation (see Fig. S6(a)) and then numerically calculate τ_a via

$$\tau_\mathrm{a} = \frac{\int_0^{600} t^* N_\mathrm{dim}(t^*)\mathrm{d}t^*}{\int_0^{600} N_\mathrm{dim}(t^*)\mathrm{d}t^*} \approx 162.$$

Further, to determine the lifetime of dimers, we sequentially initialize 30 dimers and calculate the distance d_dim of the two particles within the dimer. When the distance is larger than the range of the alignment interaction ($d_\mathrm{dim} > 2$), the dimer counts as broken. We find that with uncorrelated noise, the typical lifetime of dimers is around $\tau_\mathrm{uc} \sim 38$, whereas for correlated noise, dimers are stable over the entire simulation (see Fig. S6(b)).

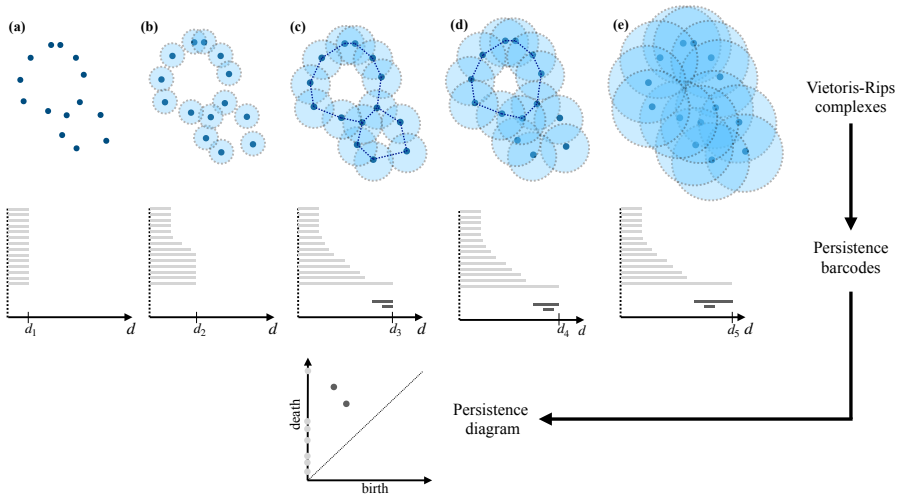

Figure S5: (a) For a small $d = d_1$ every particle itself is one connected component (H_0), born at $d = 0$. (b) For $d_2 > d_1$, some disks overlap, so some of the connected structures stop to persist, i.e. the corresponding bars in the middle row do not extend to d_2. (c) For an even larger $d = d_3$, all particles form one single connected component; thus the lower bar in light grey is the only bar that persists up to d_3 in the barcode diagram. In addition, two topological loops (H_1) have formed (dark grey bars). The left endpoints of these bars show their birth values. (d) At $d_4 > d_3$, one of these loops has disappeared (no empty space between the disks), and accordingly the lower dark grey bar ends at some value $d > d_4$, which defines the death value of the corresponding topological loop. The corresponding birth and death values are summarized in the persistence diagram. Here, the light grey dots on the death axis represent the death values of the individual connected components (H_0) and the dark grey dots show the birth and death values of topological loops (H_1). The persistence diagram is used in the main text for analyzing the network patterns. Adapted from [5].

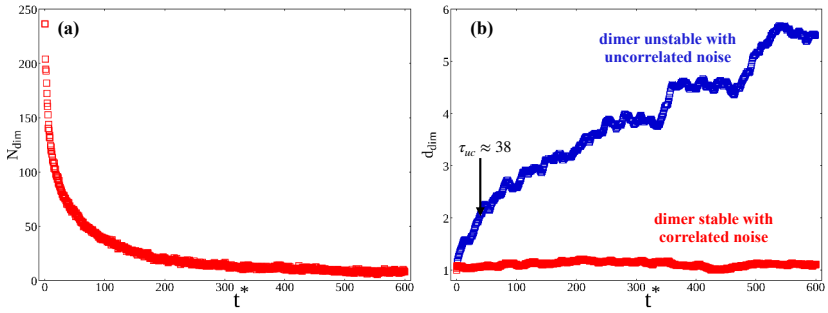

Figure S6: (a) Time evolution of the number of dimers N_{dim} in the system in the presence of correlated noise with $\alpha = 4.0$, $\omega^* = 3.0$, $\Phi_0 = 0.1$. (b) Averaged distance between two particles which initially build a dimer in the presence of uncorrelated (blue) and correlated (red) noise.

6 Movies

In all movies the following parameters are fixed: $\Phi_0 = 0.1$, $\epsilon^* = 1.0$ and $\kappa^* = 1.0$.

- Movie01-flocking: $\omega^* = 0.0$ and $\alpha = 4.0$, $a^* = 1.0$;
- Movie02-clusters: $\omega^* = 1.0$ and $\alpha = 4.0$, $a^* = 1.0$;
- Movie03-network-patterns: $\omega^* = 3.0$ and $\alpha = 4.0$, $a^* = 1.0$;
- Movie04-without-noise: $\omega^* = 3.0$ and $a^* = 0.0$

References

[1] Y. Liu, J. Li, S. Sun, and B. Yu. Advances in Gaussian random field generation: a review. Comput. Geosci., 23:1011, 2019.

[2] T. H. Beumann, A. M. Turner, and V. Vitelli. Critical and umbilical points of a non-Gaussian random field. Phys. Rev E, 88:012115, 2013.

[3] J. Carron, M. Wolk, and I. Szapudi. On fast generation of cosmological random fields. MNRAS, 444:994, 2014.

[4] M. Frigo and S.G. Johnson. The Design and Implementation of FFTW3. Proceedings of the IEEE, 93:216, 2005.

[5] F. Chazal and B. Michel. An Introduction to Topological Data Analysis: Fundamental and Practical Aspects for Data Scientists. Front. Artif. Intell, 4:667963, 2021.